The characteristics of ambient seismic noise as a source for surface wave tomography

Yingjie Yang and Michael H. Ritzwoller

Center for Imaging the Earth's Interior
Department of Physics
University of Colorado at Boulder
Boulder, CO 80309-0390
303-735-1850
yingjie.yang@colorado.edu

Abstract

In this study, we cross-correlate waveforms of ambient seismic noise between 6 and 100 sec to study the origin of ambient seismic noise. We use one year of data recorded at numerical stations located in Europe, North America, and southern Africa. We measure the signal-to-noise ratios (SNR) of Rayleigh waves for positive and negative correlation time lags at periods of 8, 14, 25 and 50 sec to determine the azimuthal distribution of strong ambient noise sources. Ambient noise at both primary (10-20 sec) and secondary microseism bands (5-10 sec) comes dominantly from the direction of nearly coastlines with stronger noise occurring in the northern hemisphere in northern winter and in the southern hemisphere in southern winter, consistent with the hypothesis that oceanic microseisms are generating this noise. The observed differences in the directivity of noise at primary and secondary microseismic bands are the consequence of propagation and attenuation, rather than the generation mechanism. At intermediate and long periods (> 20 sec), there are no appreciable seasonal variations in both signal strength and directivity. Our results are consistent with near-coastal sources rather than deep ocean sources. Even with the inhomogeneous distribution of the dominant noise sources, there is nearly azimuthally homogenous ray coverage in surface wave tomography from one year of ambient noise data.

1. Introduction

Cross-correlations of random wavefields have been shown to recover empirical Green functions between two receivers in a number of disciplines. In seismology, two types of signals can be considered to be random wavefields. The first is seismic coda, which results from the multiple scattering of seismic waves by small-scale inhomogeneities (e.g., Aki and Chouet, 1975; Paul et al., 2005). The second is ambient seismic noise. Ambient noise, in contrast with seismic coda, has the advantage that it does not depend on earthquake occurrence and can be recorded at any time and any location.

Recently, surface wave tomography for Rayleigh waves based on cross-correlations of ambient seismic noise has been applied successfully to real data at regional scales, such as in the western US (Shapiro et al., 2005; Sabra et al., 2005; Moschetti et al., 2007; Lin et al., 2007b), South Korea (Cho et al., 2006), Tibet (Yao et al., 2006), and New Zealand (Lin et al., 2007a), and at continental scales, such as in Europe (Yang et al, 2006) and North America (Bensen et al., 2007b). The basic assumption underlying ambient noise tomography is that the sources of ambient noise can be considered as random wavefields when taken over sufficient long times, such as one year. A random distribution of sources of ambient noise results in symmetric cross-correlations with strong arrivals at both positive and negative correlation lag times, usually referred to as the causal and acausal arrivals. In practice, strong asymmetry of cross-correlations is often observed, which results from inhomogeneous distributions of ambient noise sources (Derode et al., 2003). An inhomogeneous source distribution will affect the signal-to-noise ratios of the causal and acausal parts of the cross-correlation, but not the travel times, as shown experimentally by Derode et al. (2003). An inhomogeneous distribution of sources of ambient noise, however, may result from ambient noise propagating in certain preferential directions. In this case, only those station pairs oriented subparallel to these

directions will have large amplitudes and high quality empirical Green functions; whereas station pairs oriented perpendicular to these directions will have lower quality cross-correlations (Sabra et al., 2005). An inhomogeneous azimuthal distribution of inter-station paths could interfere with the ability to obtain reliable Green functions and measure dispersion curves on them. It could also limit the lateral resolution in surface wave tomography and yield smeared features along these preferred directions. Thus, a better understanding of the origin of ambient noise sources and its temporal and spatial distribution is needed to ensure that ambient noise tomography is being developed on a firm footing.

Ambient seismic noise in the short period band (< 20 s), referred to as microseisms, is related to the interaction of ocean swells with coastlines. Two strong peaks of the short-period seismic noise are observed in the primary (10-20 sec) and secondary (5-10 sec) microseism bands. The exact generation mechanism of the microseisms is not completely understood. It is commonly believed that the primary microseism involves direct interaction of ocean swells with the shallow seafloor or the shore [Hasselmann, 1963]. The secondary microseism, with double-frequency signals relative to the primary microseism, is believed to be generated by the nonlinear interaction between direct and coastline-reflected swells [Longuet-Higgins, 1950].

Long-period seismic noise, referred to as the “hum”, is observed in the continuous background free oscillations in low-frequency seismic spectra [Nawa et al., 1998]. This term is usually reserved for motions with periods above 100 sec. Early studies attributed the long-period noise to atmospheric motions (Tanimoto and Um, 1999; Ekstrom, 2001). More recent studies (Tanimoto, 2005; Rhie and Romanowicz, 2004; Rhie and Romanowicz, 2006), however, suggest that the origin of the long-period noise is more likely to be related to so-called ocean infragravity waves, a long-period ocean wave mode. Rhie and Romanowicz (2004) proposed that the generation of long-period seismic noise involves a three stage atmosphere-ocean-seafloor coupling process.

The procedure to use long-duration cross-correlations to study the long-range correlation properties of ambient seismic noise was developed by Stehly et al. (2006). They applied the method to about 20 stations in each of California, the eastern US, Europe, and Tanzania and found that ambient noise in the secondary microseism band is seasonally stable and emerges predominantly from nearby coastlines, presumably due to the interaction of ocean swell with the coast. In contrast, the primary microseism and longer period ambient noise (below 40 sec period) vary seasonally in similar ways. This observation appeared to them to sever the physical link between the primary and secondary microseisms, and called into question the commonly believed casual relation between these waves. These authors argue that the cause of the primary microseism and the longer period ambient noise is ocean wave activity in deep water. This conclusion is at variance with the study of Rhie and Romanowicz (2006), which is based on detailed observations performed on seismic arrays in Japan and California during a large storm in the Pacific. They conclude that at all periods, from the secondary microseism at several seconds period to earth hum at 240 sec, ocean wave energy is coupled to the solid earth predominantly near coastlines. They argue that nonlinear ocean wave-wave interactions near the coast generate long period energy, which propagates globally both as seismic waves in the solid earth and infragravity waves in the ocean which can then liberate there energy to the solid earth later, elsewhere. This mechanism implies that ambient noise is not uniformly distributed in time or space, which may vitiate assumptions that underlie ambient noise tomography.

In this study, we follow the methodology of Stehly et al. (2006), but apply the method to a much larger station set in Europe, North America, and southern Africa using 12 months of ambient noise data over a broad period band from 6 to 100 sec, which covers the microseism band as well as long-period noise. By analyzing the strength and quality of the cross-correlations in different seasons, directions, and period bands, we address three principal questions. First, we consider whether the primary and secondary

microseisms behave differently and, hence, may be physically decoupled. Second, we ask whether the observations are consistent with generation in shallow coastal waters at all periods or appear to require a deep-water source at long-periods. Finally, we consider whether the resulting azimuthal distribution of ambient seismic noise is sufficiently homogeneous when taken over long times for ambient noise tomography to be successful. We focus on Rayleigh waves, so the results for Love waves may differ.

2. Initial analysis: Cross-correlations of noise in Europe

We collected continuous vertical-component seismic data from ~125 stations from the Global Seismic Network (GSN) and the Virtual European Broad-Band Seismic Network (VEBSN) (Figure 1) over the 12 months of 2004. The data processing procedure applied here is similar to that described at length by Bensen et al. (2007a). Raw seismic data are processed one day at a time for each station after being decimated to 1 sample per second, and are band-pass filtered in the period band from 5 to 100 sec after the daily trend, the mean and the instrument response are removed. Filtered daily data are then normalized in time and whitened in this frequency band to remove earthquake signals and instrumental irregularities prior to performing cross-correlation. Daily cross-correlations are computed between all station-pairs and then stacked to produce two five-month and one one-year time series. The two five-month stacks are centered on January and July respectively; namely, months 11,12, 1, 2, 3 and months 5,6,7,8,9. The five-month stacks are used to investigate the seasonal variability of ambient noise source.

Examples of 12-month cross-correlations are plotted in Figure 2 with the corresponding path segments shown in the bottom map. For each cross-correlation, surface wave signals coming from the two opposite directions between the two stations appear at positive (casual component) and negative (acausal component) correlation time lag, respectively. The incoming directions of seismic noise contributing to positive components are marked with arrows along each path segment in Figure 2f. The positive

components are for waves coming mostly from the northerly direction. The amplitude of the causal and acausal components depends on the strength and density of sources of ambient noise in line with the stations. Although signals coming from opposite directions sample the same structure between a station pair, the source characteristics, such as distance, strength, duration, density, frequency content and so on, may be very different on the two opposite sides. Thus, the resulting cross-correlations are often asymmetric, as illustrated in Figure 2, and these properties may be period dependent. For example, the higher amplitude arrivals in Figure 2 are generally from the north; i.e., at positive lag. The negative components for station-pairs ECH-TUE and DSB-TUE are nearly flat, indicating that there is relatively little energy arriving from the southeast. There is, however, substantial energy at negative lags for the pairs GRFO-TUE, MORC-TUE and KWP-TUE, resulting from waves coming from the southwest. There is also apparently a difference in frequency content at positive and negative lags. The best example is probably MORC-TUE, where a clear low frequency precursor appears at positive lag (coming from the northeast), which is missing at negative lag.

To demonstrate the frequency content of the signals in Figure 2, we plot in Figure 3 normalized amplitude spectra of the positive (right) and negative (left) components of the corresponding cross-correlation time-series. In each case, 1000-second time series are used to compute the spectrum, starting from the origin time. The lower curve in each panel is the normalized spectrum of trailing noise contained in the 1000 sec time window starting at 1000 sec lag time, which is always well removed from the surface wave signals. To investigate the frequency-dependent characteristics of ambient noise sources, we divide the entire frequency band into three sub-bands: namely, LFN (0-0.05 Hz), MS1 (0.05-0.1 Hz) and MS2 (0.1-0.2 Hz), which corresponds to low frequency noise (20-100 sec), the primary microseism (10-20 sec) and the secondary microseism (5-10 sec), respectively. For cross-correlations between station pairs of GRFO-TUE, MORC-TUE and KWP-TUE, there are strong low frequency noise signals in the positive components

(Fig. 2b,c,d; and Fig. 3d,f,h), which come from the northeast quadrant (Fig. 2f). For the cross-correlations ECH-TUE and DSB-TUE, strong microseismic noise signals are observed in the positive components (Fig. 2a,e; and Fig. 3b,j), coming from the northwest quadrant, but little energy is observed in the LFN band. The lack of high-frequency noise from a particular direction probably is a consequence of a distant source. The frequency-dependent characteristics of noise signals in strength and incoming direction are discussed in more detail in the next section.

To evaluate the quality and amplitude of the cross-correlations quantitatively, we calculate the period-dependent signal-to-noise (SNR) for the positive and negative components of each cross-correlation. SNR is defined as the ratio of the peak amplitude within a time window containing the surface wave signals to the root-mean-square of the noise trailing the signal arrival window. The signal window is determined using the arrival times of Rayleigh waves at the minimum and maximum periods of the chosen period band (6 to 100 sec) using the global 3-D shear velocity model of Shapiro and Ritzwoller (2002). Period dependence of SNR is determined by applying a series of narrow band-pass (ranging form 5 to 10 mHZ) filters centered on a grid periods from 6 to 100 sec. Figure 4a shows an example of a symmetric component (average of positive and negative lags) broadband cross-correlation along with seven narrow band-pass filtered time series. Rayleigh wave signals show up clearly in each of these bands. Figure 4b displays the corresponding SNR as a function of period. SNR in this example (and generally) peaks in the primary microseism band (10-20 sec), around 14 sec period.

3. Sources of ambient noise observed in Europe

To begin to investigate the directions of the incoming ambient noise systematically, we plot the azimuthal distribution of SNR for the positive and negative components of each cross-correlation at 8, 14, 25 and 50 sec period in winter and summer in Figure 5. In each case, the line points in the direction from which the energy arrives (i.e., it points to

the source) and its length is proportional to the SNR. At 8 and 14 sec period, lines drawn to the edge of circle represent a SNR of at least 80, and at 25 sec and 50 sec the lines to the circle's edge mean the SNR is at least 60.

The periods of 8 and 14 sec are near the center of the secondary (5-10 s) and primary (10-20 sec) microseism bands, respectively. The strength and directionality of ambient noise at these two periods are shown in Figure 5 to be nearly identical to one another, and they demonstrate similar, strong seasonal dependence with much stronger noise arriving in the northern winter than in the northern summer. The seasonal variation in the strength of ambient noise, with the noise level being much higher in winter than in summer, is consistent with higher sea states in winter than in summer in the north Atlantic (Webb, 1998). In the winter, at both periods the strongest energy is arriving from the northwest quadrant. The strongest arrivals are also from the northwest quadrant during the summer, but the arrivals from the north are less energetic. The one exceptional difference between the patterns of energy arrival at 8 and 14 sec is strong noise from the northeast at 14 sec during the northern summer.

The patterns of energy arriving at the longer periods of 25 and 50 sec period are quite distinct from waves in the microseism band. These waves display little seasonal variability and the azimuthal patterns of energy arriving at these periods are very similar, with the strongest energy arriving from the northeast at both periods and seasons. The only appreciable difference between 25 and 50 sec is that the SNR at 25 sec is higher than at 50 sec period.

Figures 6 and 7 illustrate possible source locations by back-projecting a great-circle arc for each station-pair with a SNR > 20. In the microseism shown in Figure 6, source directions are broadly distributed to the west and northwest of Europe. The simplest distribution of source locations would be for them to occur near the European coast, ranging from west of Spain to the European Arctic coast of the Baltic peninsula in winter. The alternative would be for the sources to emanate from a much larger area, to lie in

deep water spanning the entire North and Central Atlantic, which seems unlikely. In summer, the range of azimuths for the high SNR sources diminishes to coastal France, England, the North Sea region, and coastal Norway. In addition, at 14 sec period during the summer, energy arrives to Europe from the northeast, apparently having emanated from east of Asia. Again, the simplest explanation would be for the sources to occur along the east Asian coastline, predominantly off of China. The sole significant difference between 8 and 14 sec period is these arrivals from the Chinese coast at 14 sec during the summer. We believe that this is a propagation phenomenon, with the 8 sec waves having been attenuated more than those at 14 sec.

At 25 sec and 50 sec, illustrated in Figure 7, the patterns of the back-projected rays are nearly identical with each other and in summer and winter. The strongest arriving energy is from the northeast, probably having originated along the western Pacific coast-lines. There are also large amplitude arrivals from the western quadrants, proably having originated near the European coast.

Our analysis of ambient noise directionality in Europe indicates little significant difference between the directional content of energy arriving in the two microseism bands. The differences that do exist can be attributed to the fact that primary microseismic energy propagates farther than secondary microseismic energy. In addition, the principal of simplicity argues for near-coastal source locations. However, using data from Europe alone we cannot locate noise sources unambiguously nor determine whether the results observed in Europe are similar elsewhere in the world. Thus, in the following sections, we analyze ambient noise directionality in South Africa and North America using the stations shown in Figure 8.

4. Further analysis: Cross-correlations of noise in South Africa

The stations used in this analysis are shown in Figure 8d and 12-months of data recorded in 1998 are processed. We stack daily cross-correlations into two five-month

stacks, respectively, in winter and summer. SNR is estimated for the positive and negative components of all the stacked cross-correlations at periods of 8, 14 and 25 sec. The azimuthal distribution of SNR from the South African and European stations are plotted in Figure 9 at periods of 8, 14 and 25 sec in both summer and winter.

In understandable contrast to the observations in Europe, at periods of 8 and 14 sec, ambient noise is stronger in South Africa during the northern summer (southern winter) than northern winter (southern summer) (Fig. 9a-d). Thus, at these periods, ambient noise is stronger in the local winter in most directions. The azimuthal content of noise emanating from the southern quadrants at these two periods is very similar to one another and there is little seasonal dependence. The simplest explanation is that ambient noise from the southern quadrants arrives from nearby coastlines having been generated there. Noise from the northern quadrants is different at 8 and 14 sec, however, and there is a stronger seasonal dependence. Strong noise (SNR > 60) arriving at 14 sec from the northeast, which is particularly strong in the northern summer, back-projects to the east Asian coast similar to results from the European stations (Fig. 9d). Strong noise (SNR > 40) at 14 sec arriving from the north and northwest to South Africa during the northern winter, back-projects to the northern European coasts, also similar to observations in Europe.

These observations imply that in the microseism bands in both Europe and South Africa, the ambient noise field partitions into two subsets: one for waves generated locally which appears at both 8 and 14 sec and the other for waves generated at great distances from the stations that appears predominantly only at 14 sec. For the European stations, distant sources at 14 sec are mostly along the east Asian coast-lines and for South African stations the distant sources are also in east Asia but also along northern European coast-lines during the northern winter. Thus, although the observed ambient noise wavefields differ in directional content between the primary and secondary microseism bands, the differences are due to the more efficient propagation at the longer

period primary microseism rather than being caused by differences in physical mechanism of sources.

At 25 sec period, as in Europe, there is little seasonal dependence of the directionality of ambient noise in South Africa and the azimuthal content of ambient noise at this period differs substantially with that at either 8 sec or 14 sec period. The South African noise at this period is generally of larger amplitude than in Europe. This is probably due to higher sea states in the southern hemisphere. In addition, the 25 sec azimuthal distribution is more omni-directional than in Europe. This is consistent with the source of the ambient noise occurring being near coastal along much of the African coast-line, which extends at nearly all azimuths around South Africa. This observation is at variance with a deep water source to ambient noise at this period.

5. Further analysis: Cross-correlations of noise in North America

We have also collected continuous seismic data from numerous stations in California, the eastern US, Alaska and northwest Canada and have processed them using the same methods as for the European and South African data. Results are presented at 8, 14, and 25 sec in Figure 10.

At 8 and 14 sec period, results for the stations in the eastern US and Alaska/Canada are straightforward. SNR is larger in the northern winter than the northern summer, but the directional dependence of noise is largely seasonally independent. In addition, the directional patterns at these periods are largely similar. In Alaska and northern Canada, ambient noise at these periods arrives mainly from the south, presumably along the Pacific coast of Canada and Alaska. In the eastern US, in contrast, ambient noise arrives mainly from the northeast and west; i.e., either from the Canadian Atlantic coast or the Pacific coast of North America. Thus, at these locations there is no evidence of significant differences in the source locations at 8 and 14 sec period.

At the microseismic periods in California, the results are somewhat more complicated, however. At 8 sec, there is little seasonal variability, but at 14 sec the seasonal variation is strong and the 8 sec and 14 sec azimuthal patterns differ from one another. In the northern winter, the strongest signals arrive to California from the northwest and northeast at 14 sec, presumably arriving from the northern Pacific and northern Atlantic coasts of North America. In the northern summer, however, the strongest arrivals are from the south and southwest. These patterns are different from those at 8 sec period, in which the dominant arrivals are in the southwest quadrant throughout the year, similar to the azimuthal distribution at 14 sec period during the northern summer. Stehly et al. (2006) argue from a similar observation for the physical decoupling of the primary and secondary microseisms. We believe a much more simple explanation is that these arrivals at 14 sec period are coming from North American coast-lines in the North Pacific and North Atlantic which are too far to be observed well at 8 sec period.

At 25 sec across North America, the azimuthal patterns are largely seasonally invariant

Thus, from microseismic to long-period ambient noise, our results are consistent with near-coastal sources in substantial agreement with the argument of Rhie and Romanowicz (2006). The observed differences in directivity at 8, 14 and 25 sec are the consequence of propagation and attenuation, rather the generation mechanism.

5. Ray coverage from ambient noise

In most theoretical treatments of ambient noise tomography and coda wave interferometry, the assumption of a perfectly homogeneous distribution of noise sources is made (e.g., Snieder, 2004). The observed distribution of ambient noise is far from homogeneous, however, because exceptionally strong signals emanate only from a few

directions. Therefore, the question is raised (e.g., Rhie and Romanowicz, 2006) about what effect this will have on the emergence of accurate Green functions from cross-correlations of ambient noise and whether the observations can be used meaningfully to perform tomography.

We have addressed this question in previous studies (e.g., Shapiro et al., 2005; Yang et al., 2007; Lin et al., 2007; Moschetti et al., 2007; Bensen et al., 2007) with several lines of evidence. We showed that the observed inter-station Green functions are similar to earthquake signals when earthquakes occur near to one of the stations, that dispersion curves are seasonally repeatable even though ambient noise characteristics may change substantially, and that the dispersion curves are consistent with one another even when azimuths are quite different. In addition, we have shown that the resulting group and phase velocity maps reproduce geological structures faithfully. These and other reasons help to establish the veracity of ambient noise tomography. It should be borne in mind, however, that considerable efforts are exerted in processing ambient noise data to identify bad measurements (more than half of all observations), some of which result from low signal levels or incomplete constructive/destruction interference in the generation of the observed Green functions.

The veracity of ambient noise tomography appears, however, to be in conflict with the existence of narrow azimuthal ranges with extraordinarily large amplitudes of ambient noise (e.g., Figure 11a-c). Figure 11d-f, which presents histograms of the number of 12-month inter-station cross-correlations with SNR > 10 on either the positive or negative component, illustrates why this is not contradictory. The reason is that signals with SNR > 10 emerge from a wide range of azimuths. Only the very strongest signals are azimuthally limited. Thus, although there are preferred directions, predominantly at very short periods, sufficient ambient noise signals exist at most azimuths to allow the retrieval of meaningful Green functions.

Figure 11g-i provides insight into why ambient noise tomography works so well. It

presents bearing angles of path segments for the selected cross-correlations at 10, 16 and 30 sec. Bearing angles are defined only between -90^{o} and 90^{o} in azimuth because, for any cross-correlation, positive and negative components with noise coming from two opposite directions have the same bearing angel. Although there is a slight preponderance of paths striking northwest-southeast across Europe, particularly at short periods, the distribution is strikingly homogeneous, which is good for resolution in surface wave tomography especially for extracting information about azimuthal anisotropy. It is true that the highest SNR observations will come from only a limited azimuth range, but this will affect only the quality of the measured dispersion. In particular, in the microseism band the best measurements will be those with a northwest-southeast path, but measurements at all azimuths exist. This observation confirms the advantage of ambient noise in providing homogenous ray coverage in surface wave tomography.

6. Conclusions

Cross-correlations of ambient noise in five different regions of the world demonstrate that, from the microseismic to the long-period band, ambient seismic noise is generated predominantly along coastlines where ocean waves interact with shallow continental shelves. However, due to the large difference in attenuation at short and long periods, observed noise is dominated by the sources from nearby coastlines in the microseism bands; whereas noise at long periods has equivalent contributions from both regional and global coastline sources. Microseismic noise has more significant seasonal variability than long-period noise with stronger noise in the northern hemisphere in north winter and in the southern hemisphere in southern winter. The anisotropic distribution of noise sources results in asymmetric cross-correlations. Using one year of noise data, nearly azimuthally homogenous ray coverage can be achieved from cross-correlations even with uneven distribution of noise source, which is important for lateral resolution

and resolving azimuthal anisotropy in ambient noise tomography.

Acknowledgments

The data used in this research were downloaded from the continuous ftp database of the Orfeus (Observatories and Research Facilities for European Seismology) Data Center and from the IRIS Data Management Center. In particular, the authors are deeply grateful to the data contributors to the Virtual European Broadband Seismic Network (VEBSN), a partnership of more than 30 local, regional and global arrays and networks. The list of contributors is located at **http://www.orfeus-eu.org/meredian/vebsn-contributors.htm**. This research was supported by contract DE-FC52-2005NA26607 from the US Department of Energy.

References

Aki, K. and B. Chouet (1975), Origin of coda waves: source, attenuation, and scattering effects, *J. Geophys. Res.*, 80, 3322-3342.

Bensen, G.D., M.H. Ritzwoller, M.P. Barmin, A.L. Levshin, F. Lin, M.P. Moschetti, N.M. Shapiro, and Y. Yang (2007a), Processing seismic ambient noise data to obtain reliable broad-band surface wave dispersion measurements, *Geophys. J. Int.*, doi: 10.1111/j.1365-246X.2007.03374.x.

Bensen, G.D., M.H. Ritzwoller, and N.M. Shapiro (2007b), Broad-band ambient noise surface wave tomography across the United States, in preparation.

Cho, K.H., R.B. Hermann, C.J. Ammon, and K. Lee (2006), Imaging the upper crust of the Korean Peninsula by surface-wave tomography, *Bull. Seism. Soc, Amer.*, submitted.

Derode, A., E. Larose, M. Campillo, and M. Fink (2003), How to estimate the Green's function of a heterogeneous medium between two passive sensors? Application to

acoustic waves, *Appl. Phys. Lett.*, 83, 3054-3056.

Ekstro¨m, G. (2001), Time domain analysis of Earth's longperiod background seismic radiation, *J. Geophys. Res*., 106, 26,483–26,493.

Friedrich, A., F. Kruger and K. Klinge (1998), Ocean-generated microseismic noise located with the Grafenberg array, *J. Seism*, 2,47-64.

Fukao, Y., K. Nishida, N. Suda, K. Nawa, and N. Kobayashi (2002), A theory of the Earth's backgroud free oscillations, *J. Geophys. Res.*, 107,2206, doi:10.1029/2001JB000153.

Hasselmann, K. (1963), A statistical analysis of the generation of microseisms, *Rev. Geophys*., 1, 177–210.

Lin, F., M.H. Ritzwoller, J. Townend, M. Savage, S. Bannister, Ambient noise Rayleigh wave tomography of New Zealand (2007a), *Geophys. J. Int.*, 18 pages, doi:10.1111/j.1365-246X.2007.03414.x.

Lin, F., M.P. Moschetti, and M.H. Ritzwoller (2007b), Surface wave tomography of the western United States from ambient seismic noise: Rayleigh and Love wave phase velocity maps, *Geophys. J. Int.*, submitted.

Longuet-Higgins, M. S. (1950), A theory on the origin of microseisms, *Philos. Trans. R. Soc. London*, 243, 1–35.

Moschetti, M.P., M.H. Ritzwoller, and N.M. Shapiro (2007), Ambient noise tomography from the first two years of the USArray Transportable Array: Group speeds in the western US, submitted to *Geophys. Res. Lett.*

Nawa, K., N. Suda, Y. Fukao, T. Sato, Y. Aoyama, and K. Shibuya (1998), Incessant excitation of the Earth's free oscillations, *Earth Planets Space*, 50, 3–8.

Paul, A. M. Campillo, L. Margerin, E. Larose, and A. Derode (2005), Empirical synthesis of time-asymmetrical Green functions from the correlation of coda waves, *J. Geophys. Res.*, 110, B08302, doi:10.1029/2004/JB003521.

Rhie, J., and B. Romanowicz (2004), Excitation of Earth's continuous free oscillations by

atmosphere-ocean-seafloor

Rhie, J., and B. Romanowicz (2006), A study of the relation between ocean storms and the Earth's hum, *Geochem. Geophys. Geosyst*., 7, Q10004, doi:10.1029/2006GC001274.

Sabra, K. G., P. Gerstoft, P. Roux, W. A. Kuperman, and M. C. Fehler (2005), Surface wave tomography from microseism in southern California, *Geophys. Res. Lett.*, 32, L14311, doi:10.1029/2005GL023155.

Shapiro, N.M. and M.H. Ritzwoller (2002), Monte-Carlo inversion for a global shear velocity model of the crust and upper mantle, *Geophys. J. Int.*, 151, 88-105.

Shapiro, N.M. M. Campillo, L. Stehly, and M.H. Ritzwoller (2005), High resolution surface wave tomography from ambient seismic noise, *Science*, 307, 1615-1618.

Stehly, L., M. Campillo, N.M. Shapiro (2006), A study of the seismic noise from its long range correlation properties, *J. Geophys. Res.* 111, B10306, doi:10.1029/2005JB004237.

Tanimoto, T. (1999), Excitation of normal modes by atmospheric turbulence: source of long-period seismic noise, *Geophys. J. Int.*, 136, 395-402.

Tanimoto, T. (2005), The oceanic excitation hypothesis for the continuous oscillations of the Earth, Geophys. J. Int., 160, 276–288.

Tanimoto, T., and J. Um (1999), Cause of continuous oscillations of the Earth, J. Geophys. Res., 104, 28,723–28,739.

Webb, S. C. (1998), Broadband seismology and noise under the ocean, *Rev. Geophys*. 36, 105-142.

Yang, Y., M.H. Ritzwoller, A.L. Levshin, and N.M. Shapiro (2007), Ambient noise Rayleigh wave tomography across Europe, *Geophys. J. Int.*, 168, 259-274, 2007

Yao, H., R.D. van der Hilst and M.V. De Hoop (2006), Surface-wave array tomography in SE Tibet from ambient seismic noise and two-station analysis: I - Phase velocity maps, *Geophys. J. Int.*, 166, 732-744.

Figure captions

Figure 1. Broadband seismic stations in Europe used in this study, marked by red triangles.

Figure 2. Examples of some 12-month broadband cross-correlations. The bold gray line indicates the zero arrival time. Cross-correlations are ordered by intra-station distances with station names indicated in each waveform panel. Note that some cross-correlations are often asymmetric. The bottom map shows the locations of stations (white triangles) and path segments for corresponding cross-correlations with arrows marking incoming directions of noise contributing to positive components.

Figure 3. Normalized spectrums of positive (right) and negative (left) components of cross-correlations shown in Fig.2. The three frequency bands of FB1, FB2 and FB3 delineated by the bold lines correspond to the infragravity band, primary and secondary microseism bands.

Figure 4. (a) Example of a broadband symmetric-component cross-correlation using 12-months of data between stations IBBN (Ibbenbueren, Germany) and MOA (Molln, Austria). The broadband signal (5-150 sec) is shown at the bottom panel. Other panes are narrow band-pass filtered waveforms with central periods indicated in each panel. (b) Calculated SNR values for each narrow band-passed filtered waveforms versus period.

Figure 5. Azimuthal distribution of SNR of 5-month stacks during winter (left column) and summer (right column) at periods 8, 14, 25 and 50 sec. SNR levels are indicted by the circles with values shown in each of the diagram.

Figure 6. Back-projected great-circle paths of cross-correlations at period 8 and 14sec in summer and winter with corresponding azimuthal distribution overplotted at the center of Europe. The great-circle paths indicate the approximate locations along where noise sources constructively contribute to surface wave signals in cross-correlation.

Figure 7. Same as figure 7, but for periods of 25 and 50 sec. The cross-correlations chosen to plot here are these with SNR > 20.

Figure 8. Distribution of broadband seismic stations used in these study in (a) western US, (b) the eastern of US, (c) Alaska, (d) southern Africa.

Figure 9. Azimuthal distribution of SNR of 5-month stacks during winter (left column) and summer (right column) at periods 8 (a and b), 14 (c and d), and 25 sec (e and f) in South Africa, compared with results from Europw. SNR levels in each region are indicted by the concentric circles with each one scaled in 20. curved lines in the middle panels are back-projected great-circle paths of cross-correlations aligning in the northeast direction with SNR > 60.

Figure 10. Same as Fig. 9, but for stations in the North America: California, eastern US, and Alaska/Canada.

Figure 11. Azimuthal distribution (top) and histograms (middle) of incoming directions of noise as well as histograms (bottom) of bearing angels of path segments for cross-correlations with SNR>10 at 10, 16 and 30 sec. SNR levels are indicated by dashed circles with values shown.

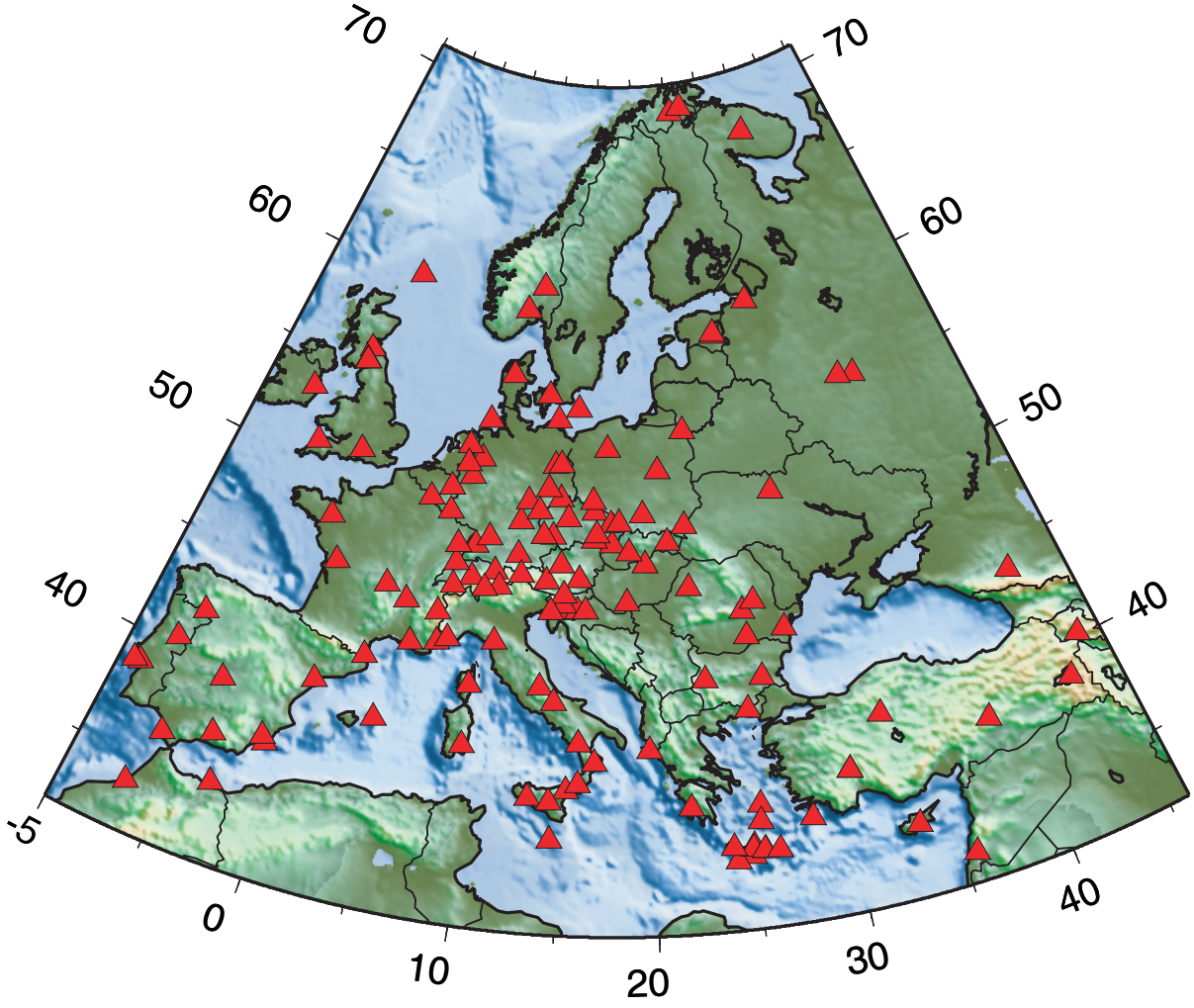
70
70
60
60
50
50
40
40
-5
0
10
20
30
40

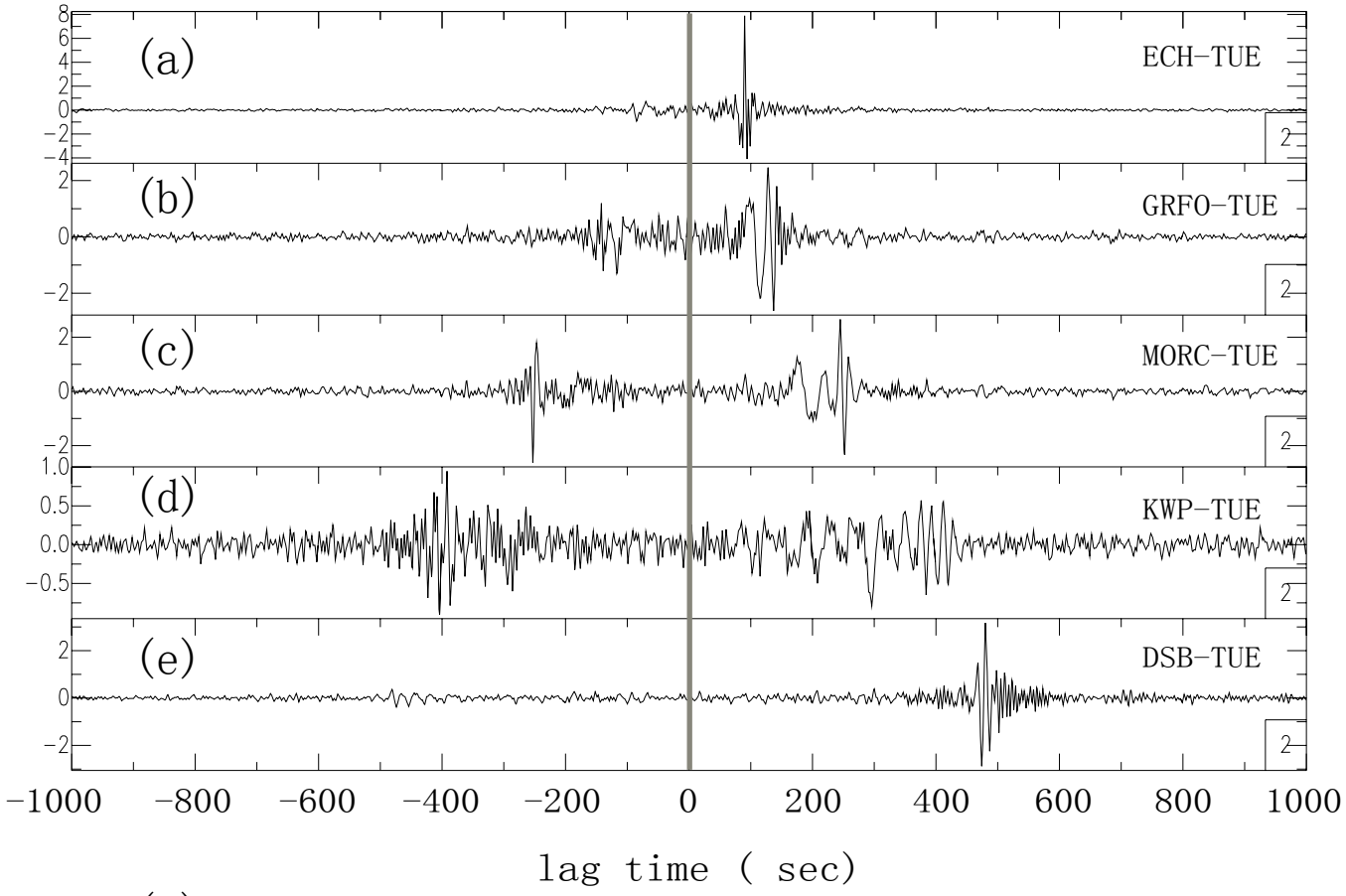
(a)
ECH-TUE
(b)
GRFO-TUE
(c)
MORC-TUE
(d)
KWP-TUE
(e)
DSB-TUE
−1000 −800 −600 −400 −200 0 200 400 600 800 1000
lag time (sec)

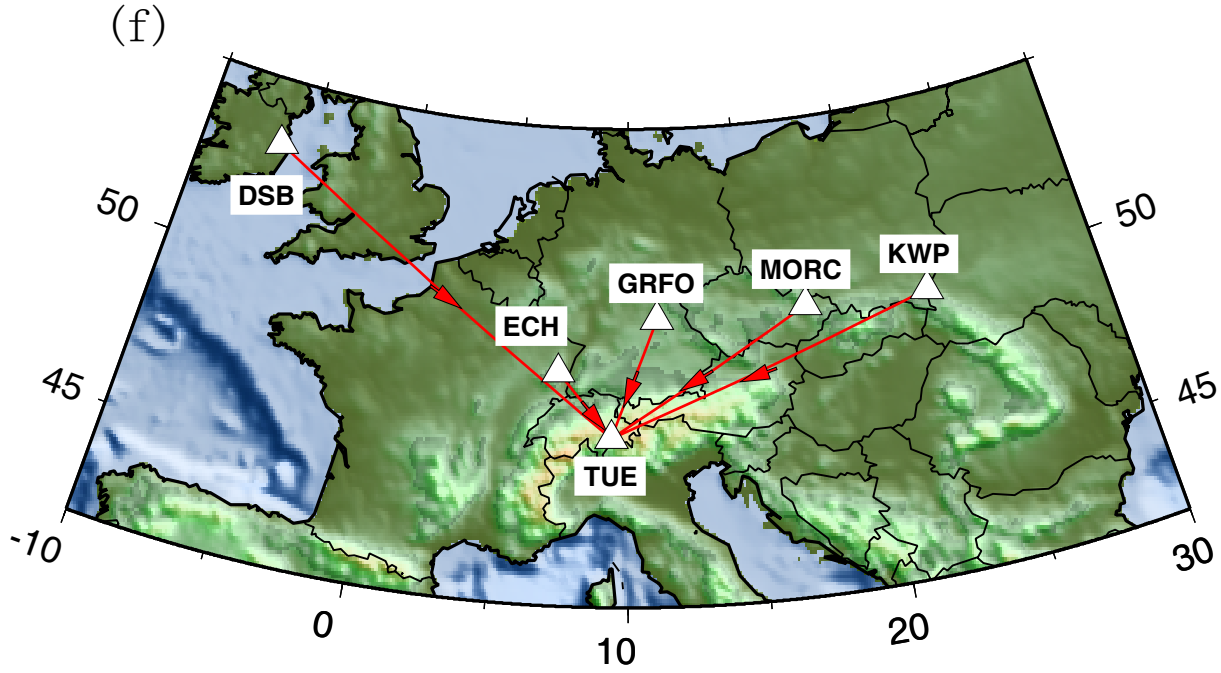
(f)
DSB
ECH
GRFO
MORC
KWP
TUE
50
45
-10
0
10
20
30

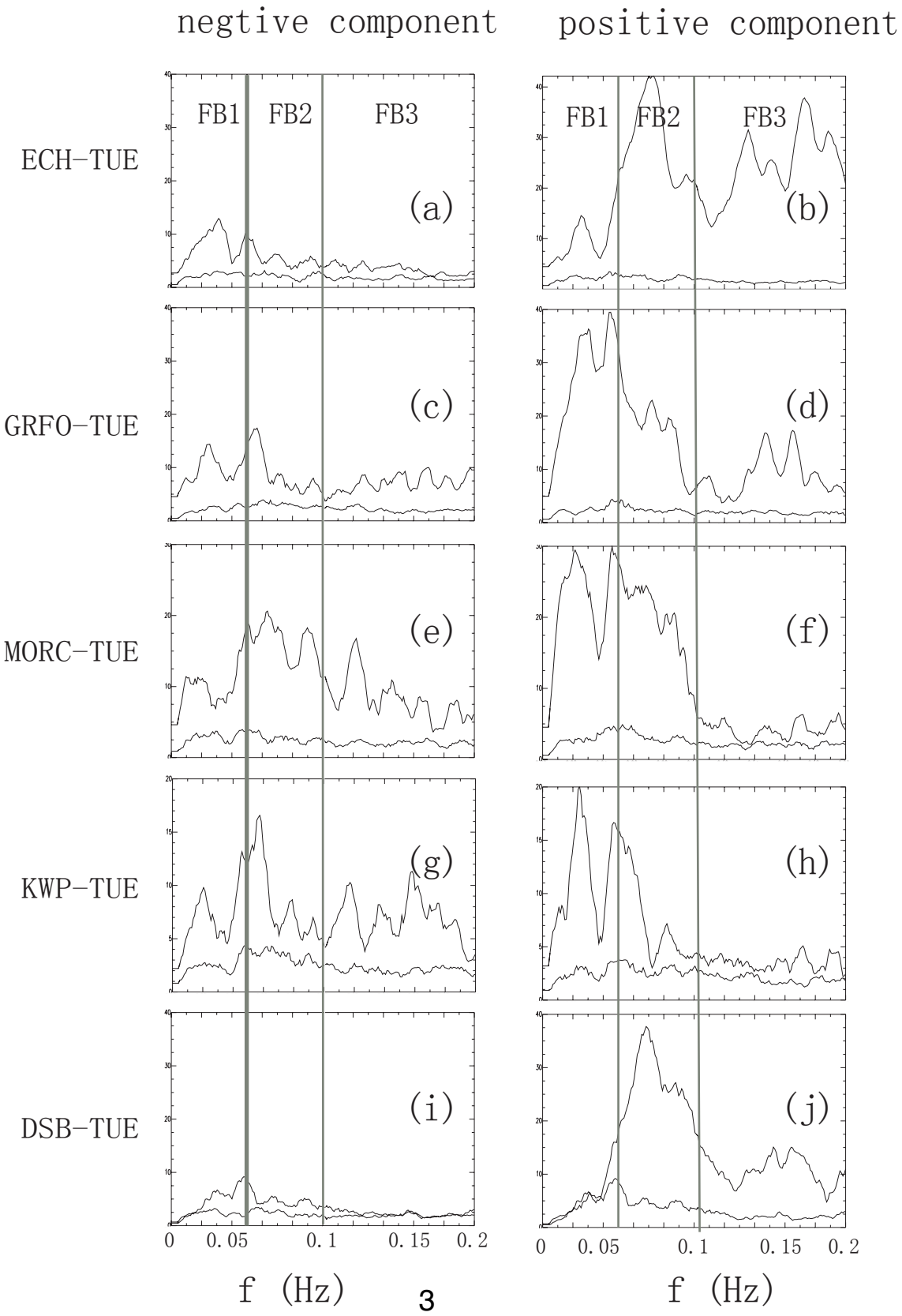
negtive component
positive component
ECH-TUE
GRFO-TUE
MORC-TUE
KWP-TUE
DSB-TUE
FB1
FB2
FB3
(a)
(b)
(c)
(d)
(e)
(f)
(g)
(h)
(i)
(j)
0
0.05
0.1
0.15
0.2
f (Hz)
f (Hz)

(a)

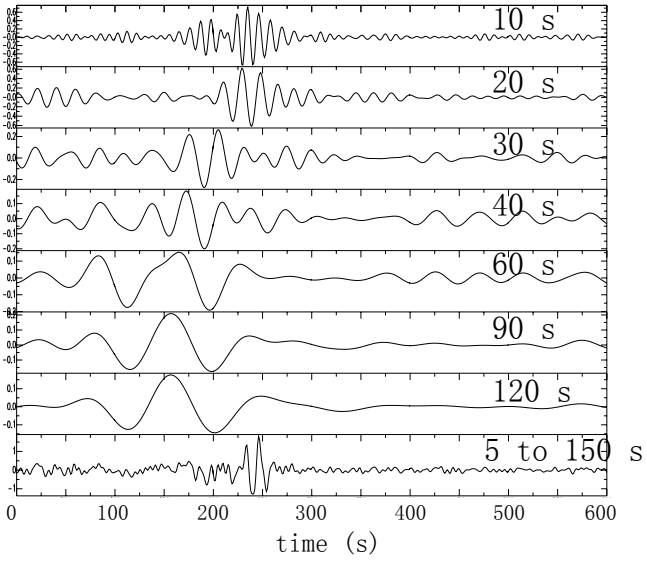
10 s
20 s
30 s
40 s
60 s
90 s
120 s
5 to 150 s
0
100
200
300
400
500
600
time (s)

(b)

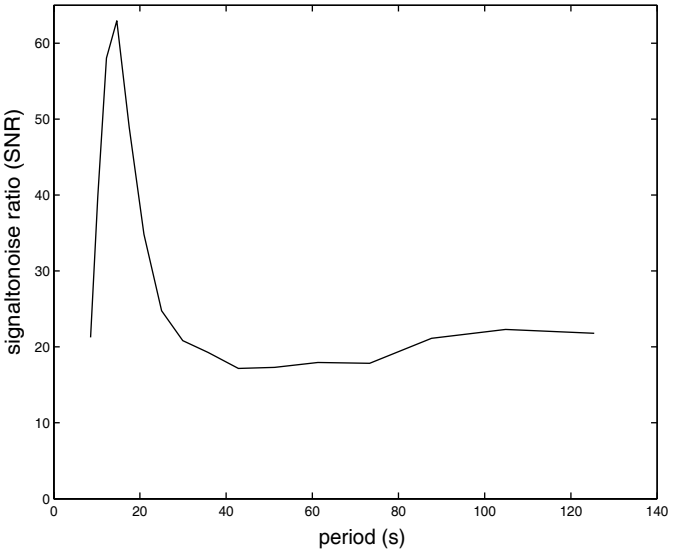
signaltonoise ratio (SNR)
0
10
20
30
40
50
60
0
20
40
60
80
100
120
140
period (s)

	northern winter	northern summer
8 sec	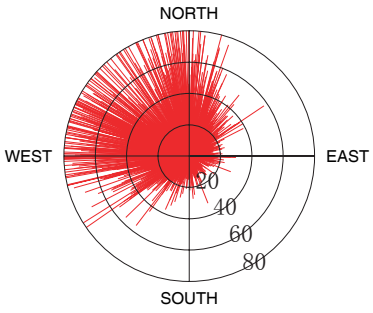	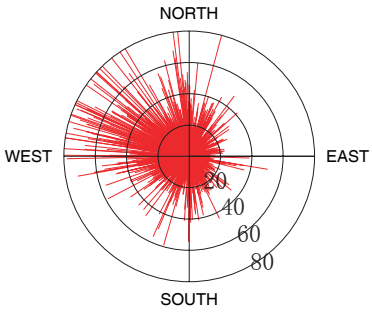
14 sec	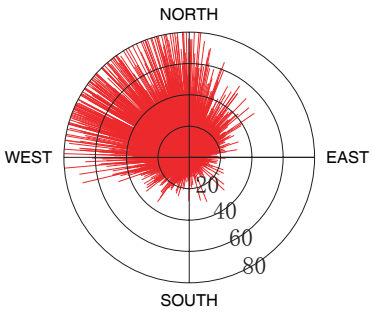	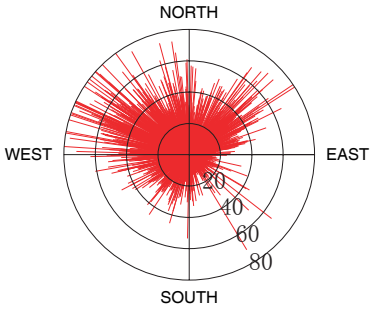
25 sec	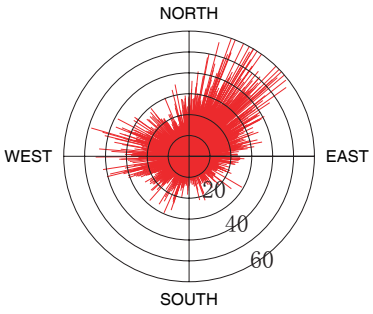	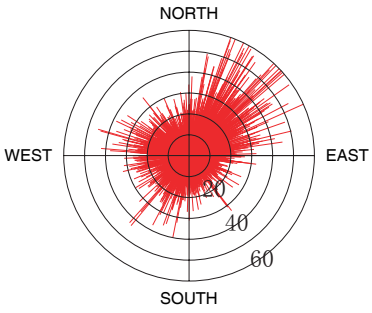
50 sec	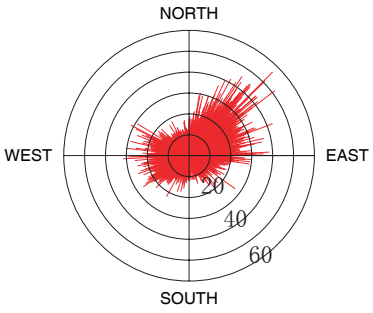	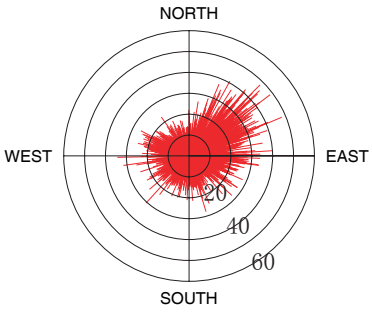

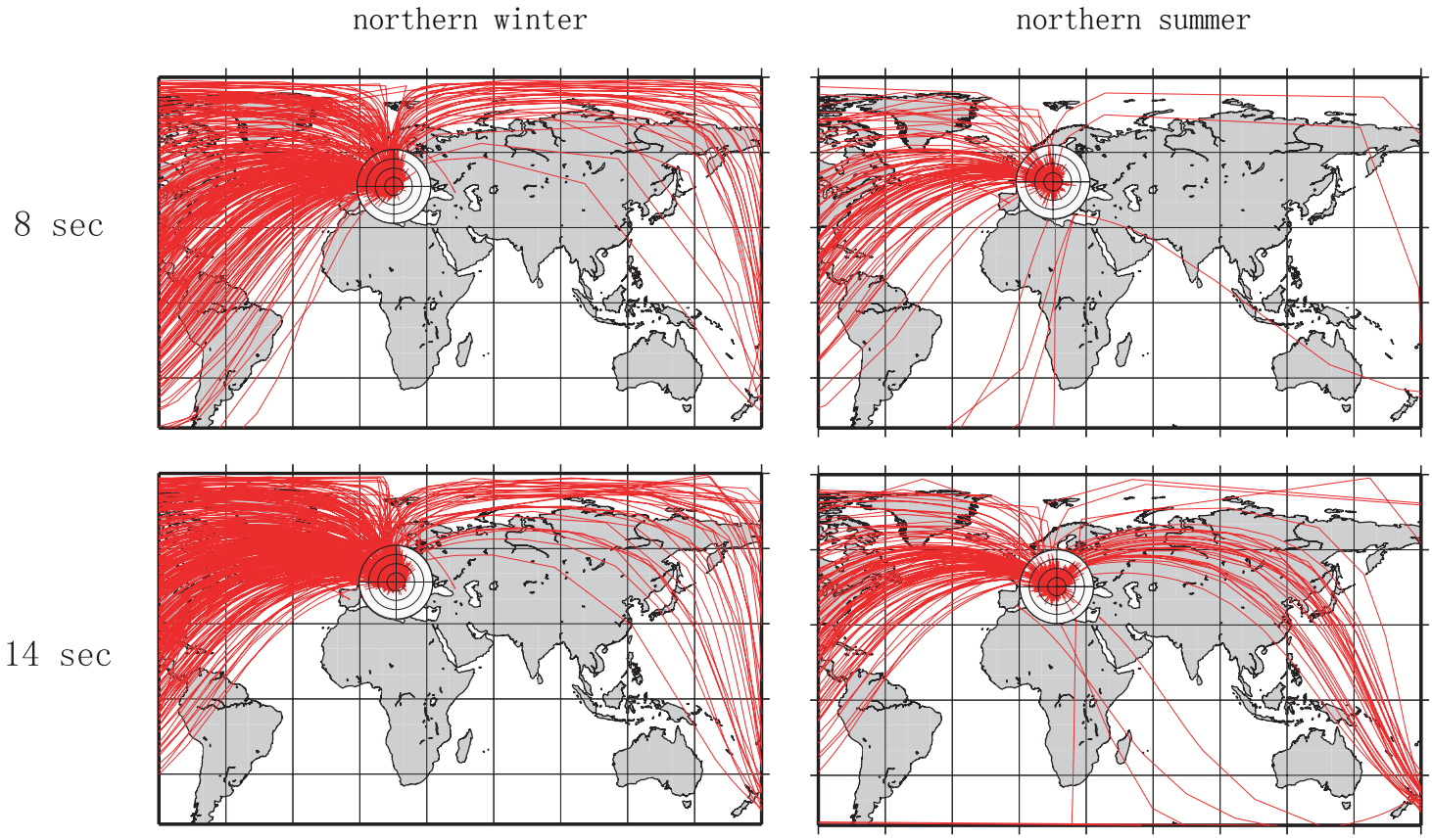
northern winter
northern summer
8 sec
14 sec

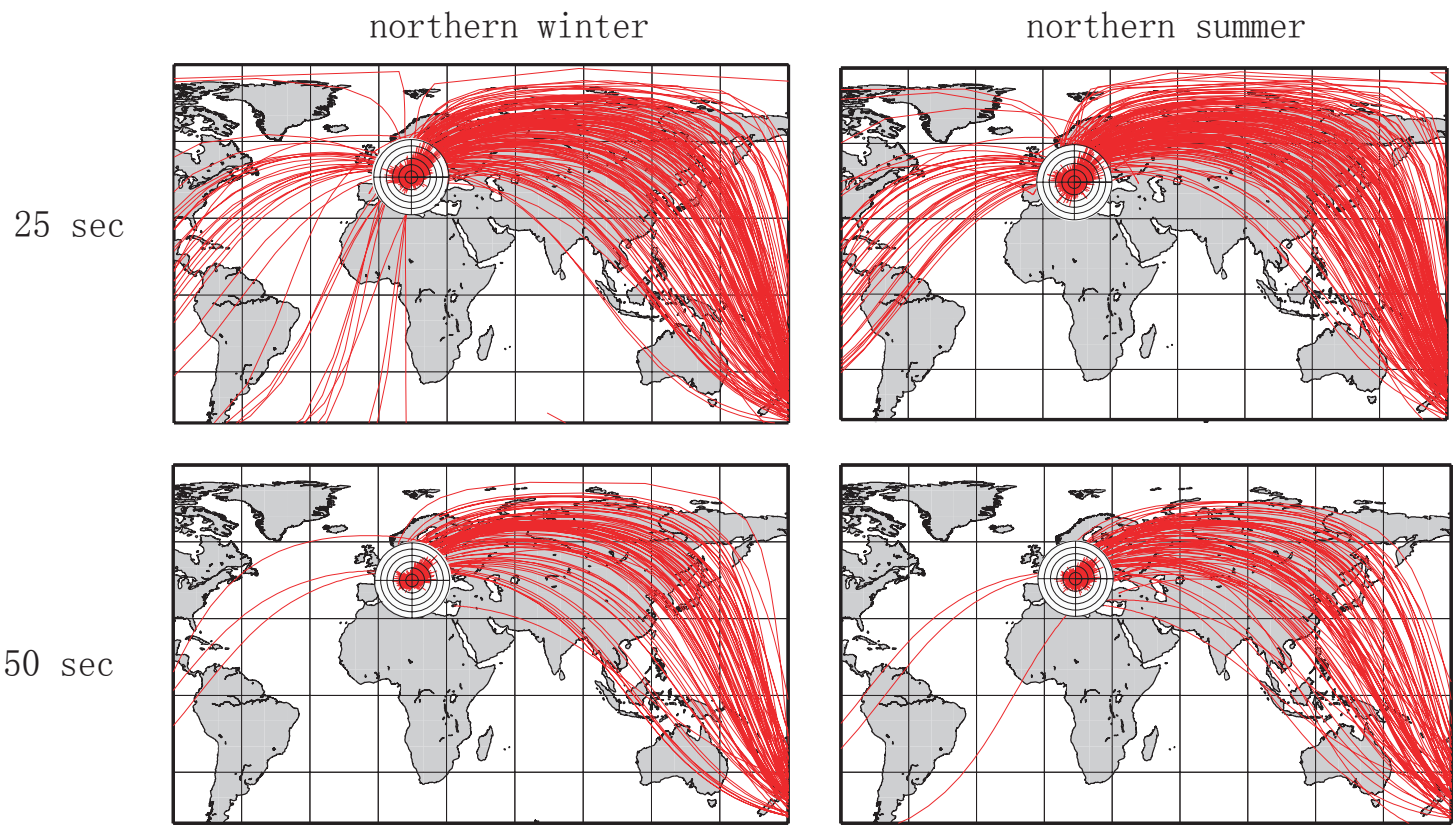
northern winter
northern summer
25 sec
50 sec

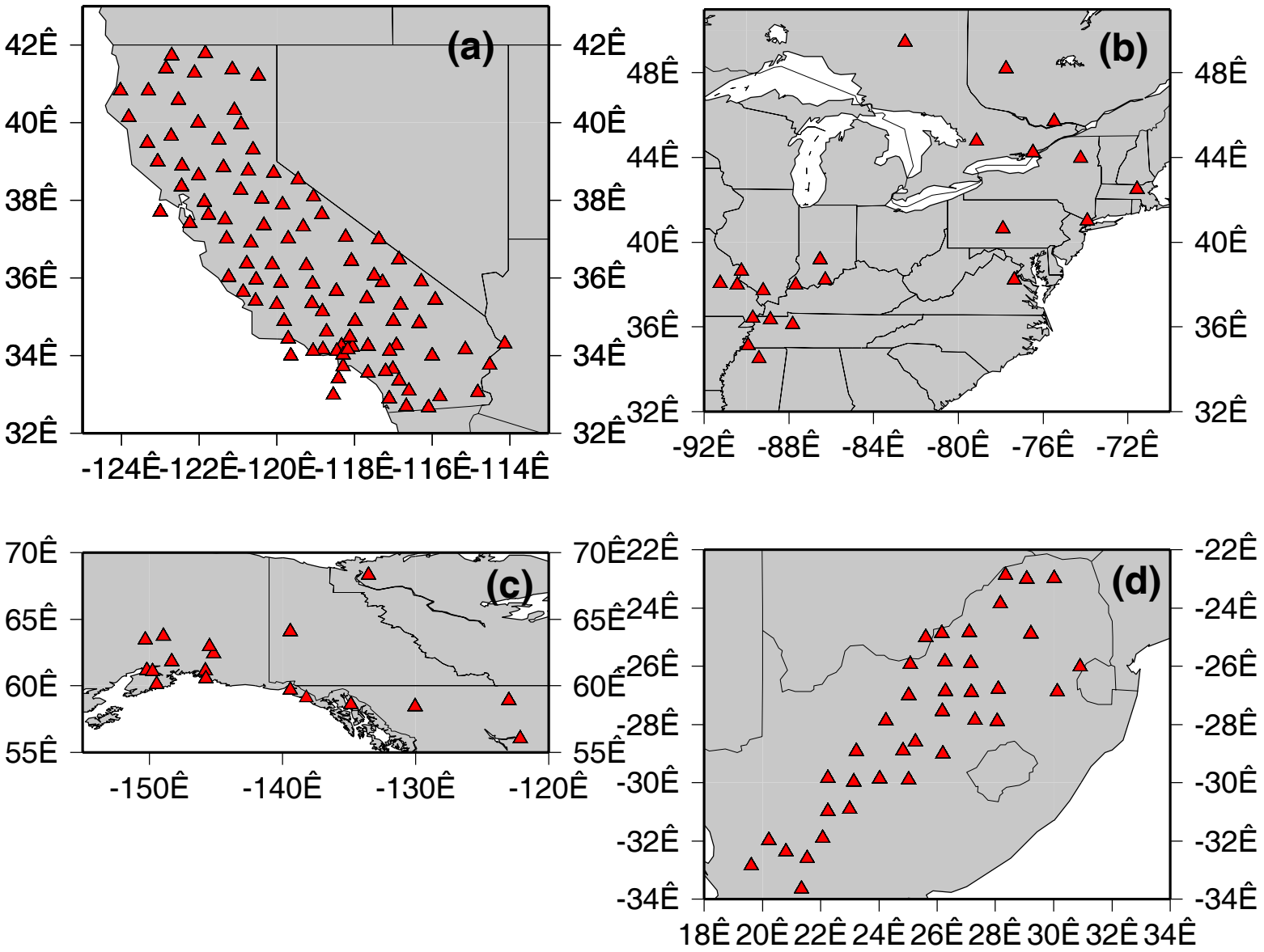
(a)
42Ê
40Ê
38Ê
36Ê
34Ê
32Ê
-124Ê-122Ê-120Ê-118Ê-116Ê-114Ê
(b)
48Ê
44Ê
40Ê
36Ê
32Ê
-92Ê -88Ê -84Ê -80Ê -76Ê -72Ê
(c)
70Ê
65Ê
60Ê
55Ê
-150Ê -140Ê -130Ê -120Ê
(d)
-22Ê
-24Ê
-26Ê
-28Ê
-30Ê
-32Ê
-34Ê
18Ê 20Ê 22Ê 24Ê 26Ê 28Ê 30Ê 32Ê 34Ê

northern winter

northern summer

8 sec

14 sec

25 sec

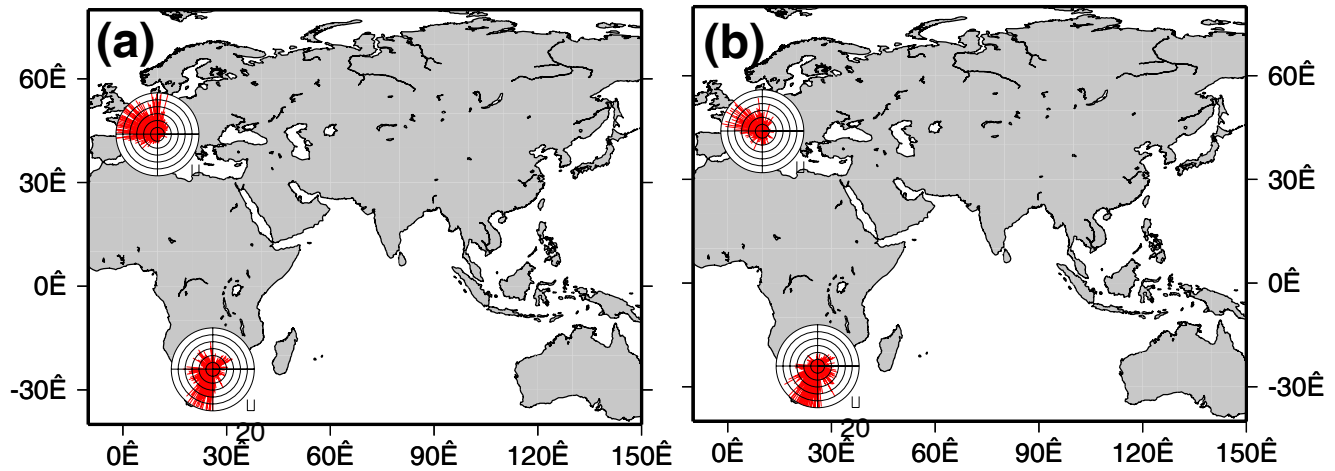

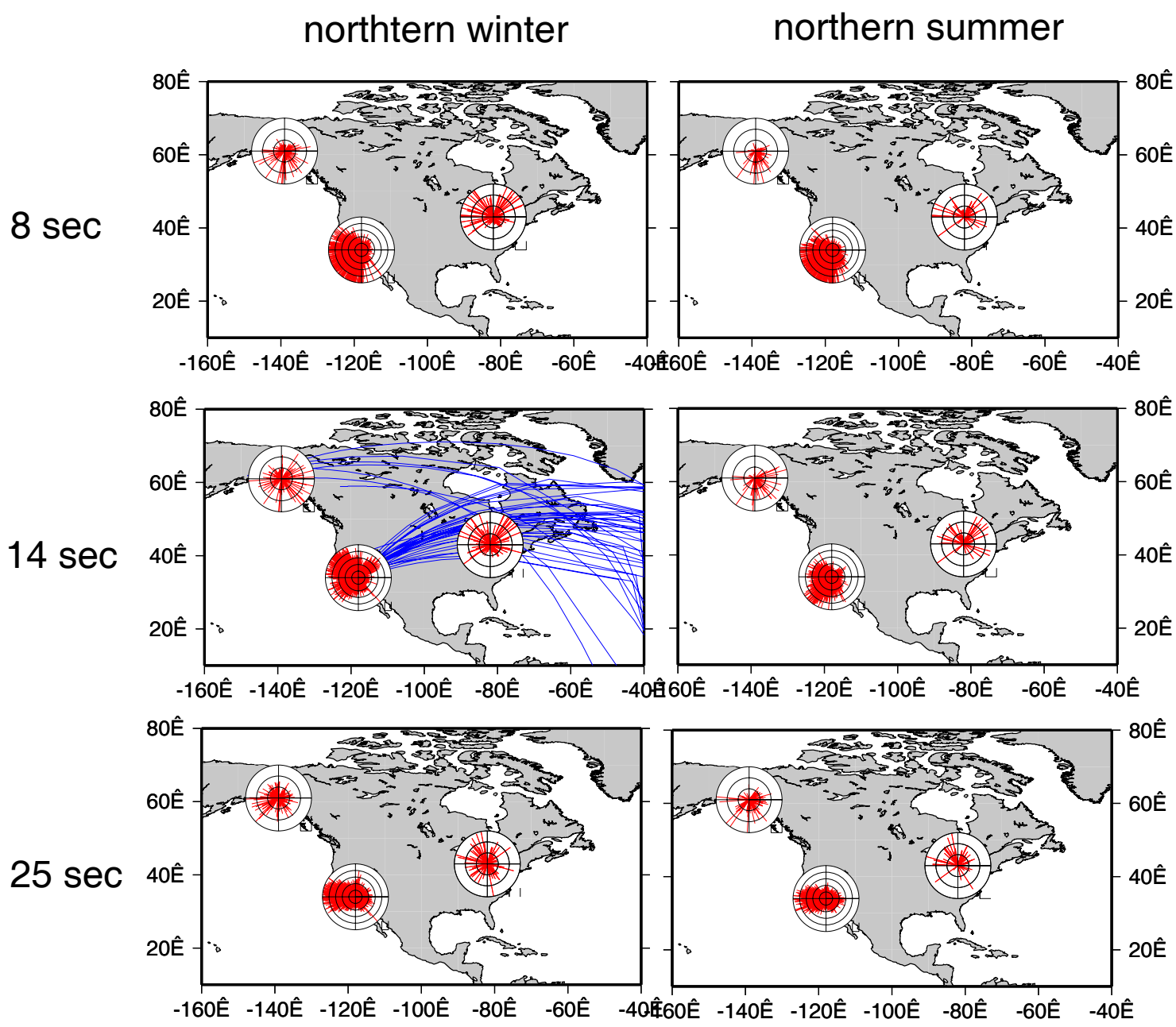
northtern winter
northern summer
8 sec
14 sec
25 sec
80Ê
60Ê
40Ê
20Ê
-160Ê
-140Ê
-120Ê
-100Ê
-80Ê
-60Ê
-40Ê

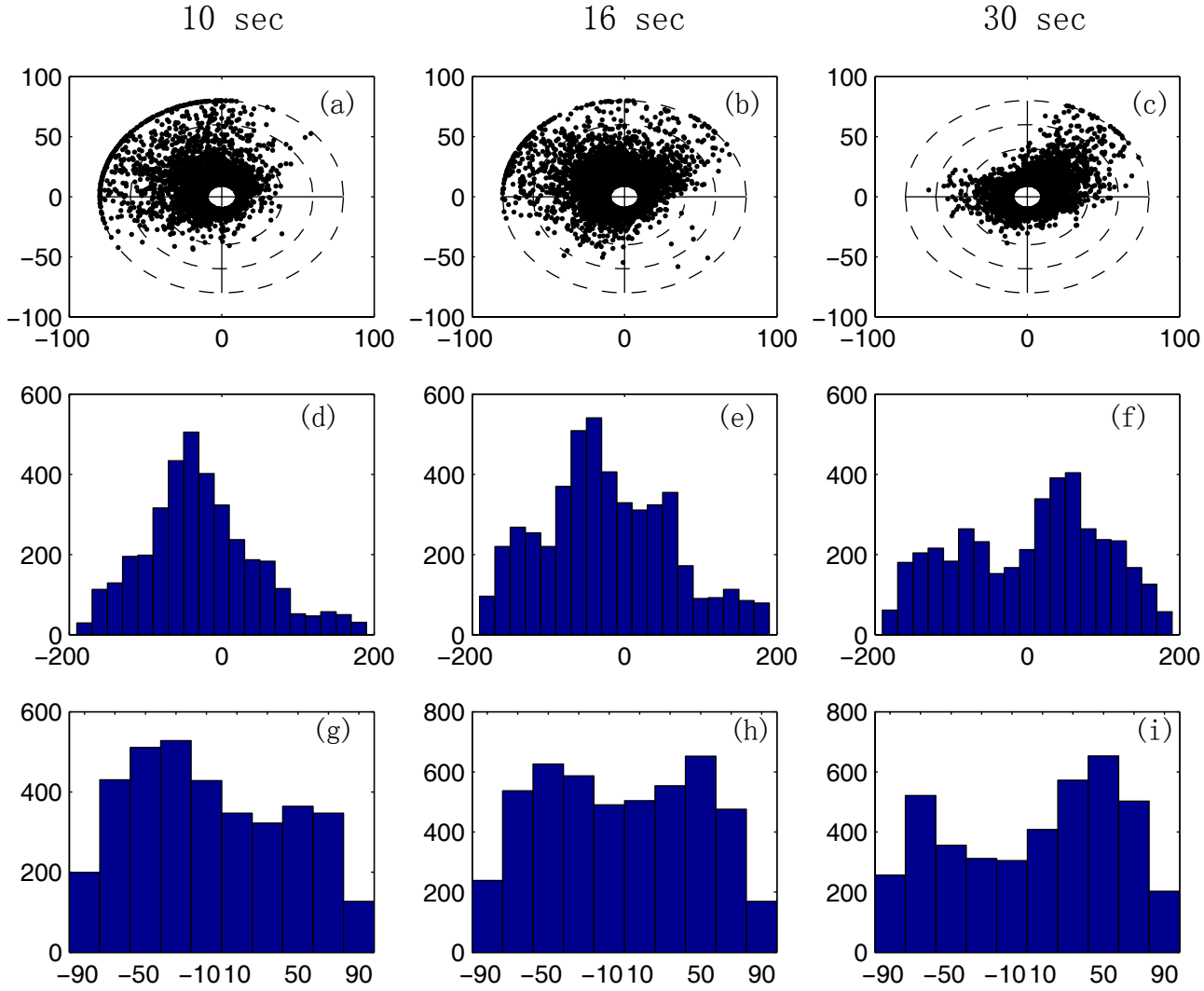
10 sec
16 sec
30 sec
(a)
(b)
(c)
(d)
(e)
(f)
(g)
(h)
(i)